A Numerically Efficient Finite-Element Formulation for the General Waveguide Problem Without Spurious Modes

JAN A. M. SVEDIN, STUDENT MEMBER, IEEE

Abstract—**A numerically efficient finite-element procedure showing no spurious modes is presented for the analysis of propagation characteristics in arbitrarily shaped metal waveguides loaded with linear materials of arbitrary complex tensor permittivity and permeability. The method is straightforwardly derived from the first-order Maxwell curl equations and comprises both the transversal and longitudinal components of the electric and magnetic fields. Hence, all necessary boundary conditions on the tangential field components are *a priori* satisfied by the trial functions. With this formulation an absence of spurious modes has been found. Furthermore, by also imposing the additional boundary conditions on the normal components of the magnetic induction and electric displacement fields, the dimension of the resulting matrix equation may be significantly reduced. In this formulation both the propagation constant and the frequency may be treated as an eigenvalue of the resulting sparse generalized eigenvalue problem. For the fundamental modes, both the convergence order and the accuracy of the presented method are found to be significantly higher than those of comparable methods when applied to some numerical examples.**

I. Introduction

THE FINITE-ELEMENT method has been widely used during the last two decades in the analysis of waveguide components [1]–[9]. With this method propagation characteristics of arbitrarily shaped waveguides of different composition are easily attainable. One drawback that has limited the use of the method, however, has been the spurious (nonphysical) solutions [1], [2], [4], [5] apparent in some of the earlier formulations of the method.

The spurious solutions satisfy the finite-element equations, but not even approximately the original boundary-value problem. The problem can be avoided by the use of a method based on the $\boldsymbol{H}$-field formulation that is modified by an enforcement of the constraint $\nabla \cdot \boldsymbol{H} = 0$ on the trial functions [7] (or an analogous $\boldsymbol{E}$-field version modified by the constraint $\nabla \cdot \boldsymbol{D} = 0$ [19]). This constraint has been empirically found to suppress the spurious modes present in this formulation. However, the inclusion of the divergence-free constraint increases the numerical complexity of the resulting eigenvalue problem by decreasing the matrix sparsity, which is important for the possibility of handling large-size problems in reasonable amounts of time and memory [4], [10]. The method has recently been generalized to lossy problems [9], but is restricted to materials with a scalar permeability, i.e., $\boldsymbol{H} \propto \boldsymbol{B}$ (or scalar permittivity for the $\boldsymbol{E}$ version, i.e., $\boldsymbol{E} \propto \boldsymbol{D}$).

A different approach, in which the spurious solutions are avoided, is formulated in terms of the transversal field components $\boldsymbol{e}_t$ and $\boldsymbol{h}_t$ [8]. Here, the spurious modes are found to possess complex propagation constants and may therefore be discriminated when considering propagating modes in nondissipative waveguides.

In this paper a numerically efficient finite-element formulation is presented that shows no spurious modes and which may be used to analyze problems involving linear materials of arbitrary complex tensor permittivity and permeability. The method is based on a mixed-field formulation [15]–[17] comprising both the transversal and longitudinal components of $\boldsymbol{E}$ and $\boldsymbol{H}$. It is straightforwardly derived from the Maxwell curl equations, and as all field components are considered, all the necessary interelement and global boundary conditions on the tangential field components $\boldsymbol{n} \times \boldsymbol{E}$ and $\boldsymbol{n} \times \boldsymbol{H}$ are easily imposed. The higher number of field components involved in this formulation does not necessarily increase the dimension of the final eigenvalue problem (for a given mesh division) as more boundary conditions may be easily imposed on the trial functions. Hence, the continuity of the normal components of the magnetic induction and electric displacement fields ($\boldsymbol{n} \cdot \boldsymbol{B}$ and $\boldsymbol{n} \cdot \boldsymbol{D}$) may also easily be imposed, which significantly reduces the final problem size.

On the other hand, in formulations showing spurious modes, some of the necessary global and interelement boundary conditions are not *a priori* satisfied by the trial functions. In fact, one reported origin of the spurious modes [2] is that some of the tangential boundary conditions, which are necessary to unambiguously define the boundary-value problem, are not satisfied. These so-called natural boundary conditions are only guaranteed to be approximately satisfied close to the physically correct solutions [11], [12], but nowhere else. Consequently, spurious solutions may occur, which are not close to any true solution and do not satisfy all the necessary boundary conditions. Two types of spurious solutions may be imagined: one type that satisfies the natural boundary conditions in a wide mean-value sense (as a sum of integrals along the boundary of each element), but pointwise unfor-

Manuscript received September 19, 1988; revised May 24, 1989.

The author is with the Department of Information Technology (F0A3), Swedish Defence Research Establishment, P.O. Box 1165, S-581 11 Linköping, Sweden.

IEEE Log Number 8930519.

tunately not even approximately [2, p. 556], and another type that does not satisfy the natural boundary conditions even in the wide mean-value sense, and hence not the Maxwell equations within each element.

Numerical examples, using both rectangular and triangular first-order elements, are given for rectangular waveguides loaded with dielectric slab, lossy dielectric, and lossy anisotropic slab and for a circular hollow waveguide. In none of these cases have spurious modes been found, and the accuracy for the fundamental modes and the convergence rate of the eigenvalue are found to be very high when compared to the magnetic-field [7], [9] and the transversal-field formulations [8]. For the first-order rectangular and triangular elements considered in this paper, $\leqslant 6N$ and between $3N$ and $6N$ unknowns are required, respectively, for N elements to be compared e.g. with exactly $8N$ and $6N$ unknowns, respectively, required in the transversal field formulation [8]. Furthermore, by matrix manipulations of the resulting eigenvalue problem, the problem dimension may be reduced up to 300 percent, but with decreased matrix sparsity as a result.

II. The Boundary-Value Problem

Consider the arbitrarily shaped metal waveguide in Fig. 1, which is composed of several different linear materials, each described by the arbitrary permittivity and permeability tensors $\hat{\epsilon}$ and $\hat{\mu}$. Taking the ordinary harmonic time dependence $e^{j\omega t}$ as understood, where ω is the real angular frequency, the source-free Maxwell curl equations are

$$\nabla \times \boldsymbol{E} = -j\omega \boldsymbol{B} = -j\omega\mu_0\hat{\mu}\boldsymbol{H} \tag{1a}$$

$$\nabla \times \boldsymbol{H} = j\omega \boldsymbol{D} = j\omega\epsilon_0\hat{\epsilon}\boldsymbol{E} \tag{1b}$$

where the vectors $\boldsymbol{E}$, $\boldsymbol{H}$, $\boldsymbol{B}$, and $\boldsymbol{D}$ are, respectively, the electric, magnetic, magnetic induction, and electric displacement field intensities, and ϵ_0 and μ_0 are the vacuum permittivity and permeability, respectively.

At the interface between two contiguous media i and j the following conditions are satisfied:

$$\boldsymbol{n} \times \boldsymbol{E}_i = \boldsymbol{n} \times \boldsymbol{E}_j \tag{2a}$$

$$\boldsymbol{n} \times \boldsymbol{H}_i = \boldsymbol{n} \times \boldsymbol{H}_j \tag{2b}$$

$$\boldsymbol{n} \cdot \boldsymbol{D}_i = \boldsymbol{n} \cdot \hat{\epsilon}_i \boldsymbol{E}_i = \boldsymbol{n} \cdot \boldsymbol{D}_j = \boldsymbol{n} \cdot \hat{\epsilon}_j \boldsymbol{E}_j \tag{2c}$$

$$\boldsymbol{n} \cdot \boldsymbol{B}_i = \boldsymbol{n} \cdot \hat{\mu}_i \boldsymbol{H}_i = \boldsymbol{n} \cdot \boldsymbol{B}_j = \boldsymbol{n} \cdot \hat{\mu}_j \boldsymbol{H}_j \tag{2d}$$

where $\boldsymbol{n}$ is the interface normal unit vector in the $x-y$ plane. On the global boundary Γ, the appropriate boundary conditions are

$$\boldsymbol{n} \times \boldsymbol{E} = 0 \tag{2e}$$

$$\boldsymbol{n} \cdot \boldsymbol{B} = \boldsymbol{n} \cdot \hat{\mu} \boldsymbol{H} = 0 \tag{2f}$$

on electric walls and

$$\boldsymbol{n} \times \boldsymbol{H} = 0 \tag{2g}$$

$$\boldsymbol{n} \cdot \boldsymbol{D} = \boldsymbol{n} \cdot \hat{\epsilon} \boldsymbol{E} = 0 \tag{2h}$$

on magnetic symmetry walls.

The classical boundary-value problem is unambiguously defined by (1a) and (1b) and the tangential boundary conditions (2a), (2b), (2e), and (2g). Solutions to these

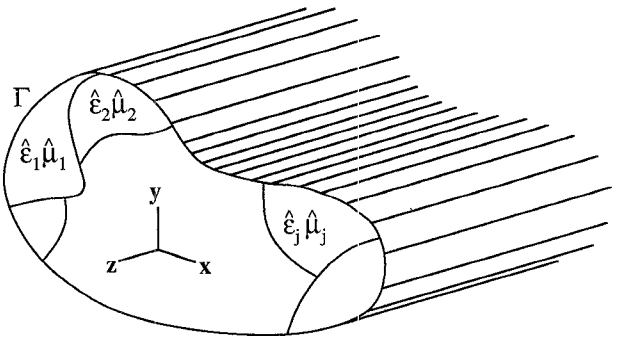

Fig. 1. The considered problem geometry, which consists of an arbitrarily shaped metal waveguide comprising several linear materials, each described by arbitrarily complex 3×3 matrices $\hat{\epsilon}$ and $\hat{\mu}$.

implicitly satisfy the Maxwell divergence equations $\nabla \cdot \boldsymbol{B} = 0$ and $\nabla \cdot \boldsymbol{D} = 0$ and the normal boundary conditions (2c), (2d), (2f), and (2h).

The presented method is based on a weak finite-element formulation of the boundary-value problem. It uses (1a) and (1b) together with an explicit pointwise enforcement of the boundary conditions (2a), (2b), (2e), and (2g) on the test and expansion functions. Boundary conditions (2c), (2d), (2f), and (2h) are also enforced (additionally) in order to reduce the size of the final matrix equation.

III. The Finite Element Formulation

In this paper, the cross section of the waveguide is divided into a number of finite elements (first-order rectangular and triangular elements are considered in the numerical examples). The six components of the electric and magnetic fields are then approximated over each element in terms of the values at each of the finite-element nodal points according to

$$\begin{pmatrix} \boldsymbol{E} \\ \boldsymbol{H} \end{pmatrix} = [N]^T \begin{pmatrix} \{E\}_e \\ \{H\}_e \end{pmatrix} e^{-j\beta z} \tag{3}$$

where $\beta = \beta' - j\beta''$ is the complex propagation constant,

$$[N] = \begin{bmatrix} Z_0\{N\} & \{0\} & \{0\} & \{0\} & \{0\} & \{0\} \\ \{0\} & Z_0\{N\} & \{0\} & \{0\} & \{0\} & \{0\} \\ \{0\} & \{0\} & jZ_0\{N\} & \{0\} & \{0\} & \{0\} \\ \{0\} & \{0\} & \{0\} & \{N\} & \{0\} & \{0\} \\ \{0\} & \{0\} & \{0\} & \{0\} & \{N\} & \{0\} \\ \{0\} & \{0\} & \{0\} & \{0\} & \{0\} & j\{N\} \end{bmatrix} \tag{4}$$

where $Z_0 = (\mu_0/\epsilon_0)^{1/2}$ is the intrinsic impedance of vacuum and

$$\{E\}_e = \begin{bmatrix} \{E_x\}_e \\ \{E_y\}_e \\ \{E_z\}_e \end{bmatrix} \qquad \{H\}_e = \begin{bmatrix} \{H_x\}_e \\ \{H_y\}_e \\ \{H_z\}_e \end{bmatrix}. \tag{5}$$

The real $k\times1$ column vector $\{N\}$ is the element shape function vector [12], where k is the number of nodal points on each element; $\{0\}$ is a $k\times1$ null vector, and T denotes a matrix transposition. The column vectors $\{E_x\}_e$, $\{E_y\}_e$, $\{E_z\}_e$, $\{H_x\}_e$, $\{H_y\}_e$, and $\{H_z\}_e$ are $k\times1$ complex field vectors representing the nodal point values of, respectively,

E_x/Z_0, E_y/Z_0, $-jE_z/Z_0$, H_x, H_y, and $-jH_z$ on each element.

The finite-element solutions $\boldsymbol{E}$ and $\boldsymbol{H}$ are weak solutions [12, ch. 4] of (1a) and (1b) which should satisfy

$$\sum_e \iint_e (\boldsymbol{E}^*_{\text{test}} \cdot (j\nabla \times \boldsymbol{H} + \omega\epsilon_0 \hat{\epsilon} \boldsymbol{E}) + \boldsymbol{H}^*_{\text{test}} \cdot (-j\nabla \times \boldsymbol{E} + \omega\mu_0 \hat{\mu} \boldsymbol{H}))\, dx\, dy = 0 \quad (6)$$

for all admissible test functions $\boldsymbol{E}_{\text{test}}$ and $\boldsymbol{H}_{\text{test}}$ where the appropriate boundary conditions are handled during the summation Σ over all elements [11]. Here, the necessary continuity requirements (2a), (2b), (2e), and (2g) on $\boldsymbol{n} \times \boldsymbol{E}$ and $\boldsymbol{n} \times \boldsymbol{H}$ are explicitly imposed, but also the additional requirements (2c), (2d), (2f), and (2h) on $\boldsymbol{n} \cdot \boldsymbol{B}$ and $\boldsymbol{n} \cdot \boldsymbol{D}$ are enforced.

Using a Galerkin procedure with the finite-element expansion (3) for both trial and test functions, there results the following generalized eigenvalue problem:

$$(\omega[P] + \beta[Q] + [R]) \begin{pmatrix} \{E\} \\ \{H\} \end{pmatrix} = \{0\} \quad (7)$$

where the column vector is composed of all the unknown nodal point parameters used to represent $\boldsymbol{E}$ and $\boldsymbol{H}$ in the waveguide and either β or ω may be treated as the eigenvalue. By writing (1a) and (1b) in component form, the quadratic sparse matrices $[P]$, $[Q]$, and $[R]$ are found to be

$$[P] = \mu_0 \sum_e \iint_e \begin{bmatrix} \epsilon_{xx}[A] & \epsilon_{xy}[A] & j\epsilon_{xz}[A] & [0] & [0] & [0] \\ \epsilon_{yx}[A] & \epsilon_{yy}[A] & j\epsilon_{yz}[A] & [0] & [0] & [0] \\ -j\epsilon_{zx}[A] & -j\epsilon_{zy}[A] & \epsilon_{zz}[A] & [0] & [0] & [0] \\ [0] & [0] & [0] & \mu_{xx}[A] & \mu_{xy}[A] & j\mu_{xz}[A] \\ [0] & [0] & [0] & \mu_{yx}[A] & \mu_{yy}[A] & j\mu_{yz}[A] \\ [0] & [0] & [0] & -j\mu_{zx}[A] & -j\mu_{zy}[A] & \mu_{zz}[A] \end{bmatrix} dx\, dy \quad (8)$$

$$[Q] = Z_0 \sum_e \iint_e \begin{bmatrix} [0] & [0] & [0] & [0] & -[A] & [0] \\ [0] & [0] & [0] & [A] & [0] & [0] \\ [0] & [0] & [0] & [0] & [0] & [0] \\ [0] & [A] & [0] & [0] & [0] & [0] \\ -[A] & [0] & [0] & [0] & [0] & [0] \\ [0] & [0] & [0] & [0] & [0] & [0] \end{bmatrix} dx\, dy \quad (9)$$

$$[R] = Z_0 \sum_e \iint_e \begin{bmatrix} [0] & [0] & [0] & [0] & [0] & -[C] \\ [0] & [0] & [0] & [0] & [0] & [B] \\ [0] & [0] & [0] & -[C] & [B] & [0] \\ [0] & [0] & [C] & [0] & [0] & [0] \\ [0] & [0] & -[B] & [0] & [0] & [0] \\ [C] & -[B] & [0] & [0] & [0] & [0] \end{bmatrix} dx\, dy \quad (10)$$

$$[A] = \{N\}\{N\}^T \quad (11)$$

$$[B] = \{N\}\partial\{N\}^T/\partial x \quad (12)$$

$$[C] = \{N\}\partial\{N\}^T/\partial y. \quad (13)$$

By solving the eigenvalue problem (7), all field components for the approximate fields of different eigenmodes in the waveguide are directly determined and the corresponding eigenvalues β (or ω) are found.

For loss-free waveguides the regular matrix $[P]$ is Hermitian and real for the usual cases, such as dielectrics and transversely magnetized ferrites. The singular matrices $[Q]$ and $[R]$ are always Hermitian.

For resonator problems or the calculation of dispersion relations in problems with frequency-independent loss-free materials, it is advantageous to treat the frequency ω as the eigenvalue, because (7) may then be reformulated as a standard eigenvalue problem, which is Hermitian. Then, very efficient sparse eigenvalue routines are available [10], [14].

The boundary conditions have been taken care of by solving (2a)–(2h) for each nodal point [18]. As an example, consider the arbitrary internal node point j (using triangular elements) shown in Fig. 2. The boundary conditions (2a)–(2h) then require the enforcement of

$$\boldsymbol{n}_t \times \boldsymbol{E}_t = \boldsymbol{n}_t \times \boldsymbol{E}_{t-1} \quad (14a)$$

$$\boldsymbol{n}_t \times \boldsymbol{H}_t = \boldsymbol{n}_t \times \boldsymbol{H}_{t-1} \quad (14b)$$

where the $\boldsymbol{E}_t$'s and $\boldsymbol{H}_t$'s represent the values of the electric

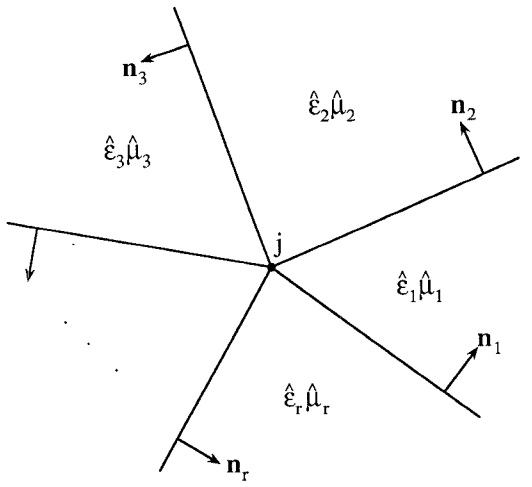

Fig. 2. The geometry at the internal node point j, in an arbitrary triangular-element mesh. Generally, the elements contain different materials, each described by constant matrices $\hat{\epsilon}_i$ and $\hat{\mu}_i$, $i=1,2,\cdots,r$.

and magnetic fields, respectively, at the node point j in the element i, and the subscript i runs cyclically modulo r from 1 to r. In this paper, the additional enforcements of

$$\boldsymbol{n}_i\cdot\hat{\epsilon}_i\boldsymbol{E}_i=\boldsymbol{n}_i\cdot\hat{\epsilon}_{i-1}\boldsymbol{E}_{i-1} \tag{14c}$$

$$\boldsymbol{n}_i\cdot\hat{\mu}_i\boldsymbol{H}_i=\boldsymbol{n}_i\cdot\hat{\mu}_{i-1}\boldsymbol{H}_{i-1} \tag{14d}$$

are also made. At the external boundary Γ one obtains similar homogeneous equations for the global boundary conditions (2e)–(2h) to be satisfied (perfect electric and magnetic conductors).

Using (14a)–(14d), it can be concluded that the total number of unknowns is $\leqslant 6N_p$, where N_p is the number of nodal points. This yields for the first-order rectangular elements $\leqslant 6N$ unknowns, where N is the number of elements. For comparison, the transversal-field method uses $8N$ unknowns for the same type of elements. For the first-order triangular elements, the required number of unknowns depends on the mean number of nodal points per triangle, but lies in the range $3N$ to $6N$, to be compared with exactly $6N$ for the transversal-field formulation [8].

To further demonstrate the difference between the method outlined here and the earlier formulations with regard to the fulfillment of boundary conditions, one should note that the dimension of the eigenvalue problem (7) may be reduced by rewriting it in terms of fewer parameters (field components). As an example, write (7) with β as eigenvalue in detailed matrix form:

$$\left(\begin{bmatrix}[P_1] & [P_2] & [0] & [R_1]\\ [P_3] & [P_4] & [R_2] & [0]\\ [0] & [R_3] & [P_5] & [P_6]\\ [R_4] & [0] & [P_7] & [P_8]\end{bmatrix} + \beta\begin{bmatrix}[0] & [0] & [Q_1] & [0]\\ [0] & [0] & [0] & [0]\\ [Q_2] & [0] & [0] & [0]\\ [0] & [0] & [0] & [0]\end{bmatrix}\right)\begin{pmatrix}\{Et\}\\ \{Ez\}\\ \{Ht\}\\ \{Hz\}\end{pmatrix}=0 \tag{15}$$

where the $[P_i]$'s, $[Q_i]$'s, and $[R_i]$'s are submatrices of $\omega[P]$, $[Q]$, and $[R]$, respectively (see the Appendix), and the column vectors $\{Et\}$, $\{Ez\}$, $\{Ht\}$, and $\{Hz\}$ are parameters used to represent, respectively, the transversal electric, longitudinal electric, transversal magnetic, and longitudinal magnetic field components for the global assembly of finite elements. Some elementary matrix algebra applied to (15) yields the following eigenvalue problem:

$$\left(\begin{bmatrix}[A] & [B]\\ [C] & [D]\end{bmatrix}+\beta\begin{bmatrix}[0] & [Q_1]\\ [Q_2] & [0]\end{bmatrix}\right)\begin{pmatrix}\{Et\}\\ \{Ht\}\end{pmatrix}=0 \tag{16}$$

where

$$[A]=[P_1]-[P_2][P_4]^{-1}[P_3]-[R_1][P_8]^{-1}[R_4] \tag{17a}$$

$$[B]=-[P_2][P_4]^{-1}[R_2]-[R_1][P_8]^{-1}[P_7] \tag{17b}$$

$$[C]=-[R_3][P_4]^{-1}[P_3]-[P_6][P_8]^{-1}[R_4] \tag{17c}$$

$$[D]=[P_5]-[R_3][P_4]^{-1}[R_2]-[P_6][P_8]^{-1}[P_7] \tag{17d}$$

which is a generalized eigenvalue problem of approximately $2/3$ the order of the original problem (7) and only comprising parameters related to the transversal field components of $\boldsymbol{E}$ and $\boldsymbol{H}$. Observe that in (16) all the necessary tangential boundary conditions are explicitly fulfilled (and additionally also the normal conditions); this is to be compared with [8], where the conditions on the longitudinal components are ignored. For all isotropic cases and the special anisotropic cases where only ϵ_{xy}, ϵ_{yx}, μ_{xy}, and $\mu_{yx}\neq 0$, the matrices $[P_2]$, $[P_3]$, $[P_7]$, and $[P_6]$ become zero with vanishing $[B]$ and $[C]$ as a result. In this case (16) may be reduced to either one of the two following eigenvalue problems:

$$\left([D]-\beta^2[Q_2][A]^{-1}[Q_1]\right)\{H_t\}=0 \tag{18a}$$

$$\left([A]-\beta^2[Q_1][D]^{-1}[Q_2]\right)\{E_t\}=0 \tag{18b}$$

each of dimension only approximately $1/3$ that of (7) and expressed in parameters related to transversal $\boldsymbol{H}$ or transversal $\boldsymbol{E}$ only. Again observe that in (18a) and (18b) all the boundary conditions on the tangential components are incorporated, and additionally also the normal conditions. Equation (18a) has been investigated, and found to produce the same eigensolutions as (7) (using the relations between the field components used to obtain (18a) from (7)).

The most important numerical property of the eigenvalue problem (7) is, however, the $O(1/N)$ sparsity of the matrices, which means that the number of nonzero matrix elements on each row is almost independent of the dimension N. For large-size problems sparse eigenvalue codes may be used on (7), which will save a significant amount of CPU time and memory [10]. As more compact forms of (7) as (16), (18a), or (18b) are less sparse, it may be preferable to use (7), despite the roughly 300 percent reduction of unknowns in, for instance, (18b).

IV. Numerical Examples

In this section examples where analytical solutions exist [13] are studied in order to demonstrate the strength of the present method. In this paper first-order rectangular and triangular elements are used. In order to easily obtain both

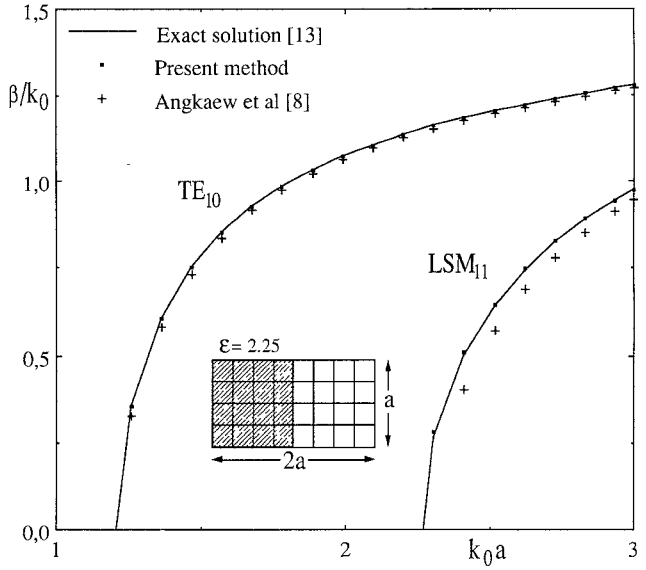

Fig. 3. The normalized dispersion relations for the fundamental TE_{10} and higher order LSM_{11} modes in the dielectric-slab-loaded rectangular waveguide (inset). The finite-element division is 4×8 for both finite-element solutions.

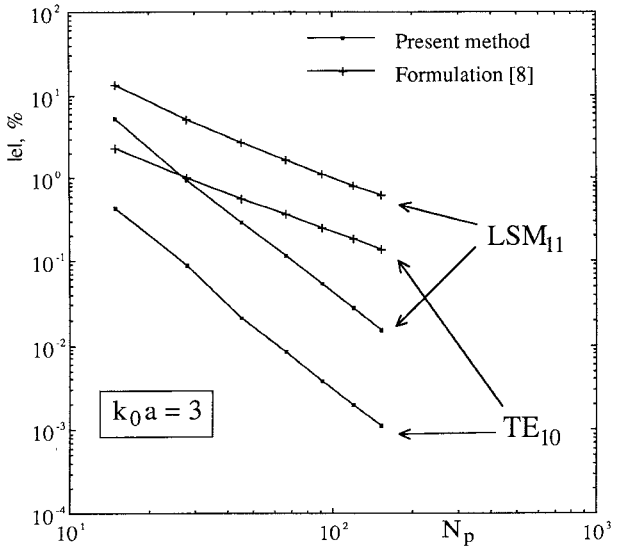

Fig. 4. The relative error, $|e|$, in the finite-element solutions of the propagation constants, β, for the modes in Fig. 3, as a function of the number of nodal points, N_p, in the finite-element mesh, using square first-order elements.

eigenvectors and eigenvalues, the complex generalized eigenvalue problem routine NAG F02GJF (in double precision) is used [14]. With this routine, all the eigenvalues and eigenvectors of (7) are given but the matrix sparsity is not considered and consequently the more compact forms (16) or (18) would probably be faster to execute despite the necessary matrix inversions involved. As pointed out elsewhere [4], [10], the use of sparse matrix routines will considerably reduce the amount of storage and computational time needed to solve (7). In fact, for very large problems, even on a supercomputer, the sparsity of the eigenvalue problem will be of decisive importance.

A. Dielectric Slab in Rectangular Waveguide

As a first example [8], a rectangular waveguide inhomogeneously loaded with a dielectric slab is considered. In Fig. 3 the calculated and exact [13] dispersion relations for the fundamental TE_{10} and the higher order LSM_{11} mode are given for a waveguide of dimensions $a\times2a$ loaded at one end with a dielectric slab of dimensions $a\times a$ and relative permittivity $\epsilon = 2.25$. The cross section was divided into $4\times8 = 32$ elements ($6\times32 = 192$ variables). For comparison, the transversal field ($\boldsymbol{e}_t - \boldsymbol{h}_t$) method [8] was coded using the same type of elements. For this structure using the same division for both methods, the present method is more accurate, as is obvious from the dispersion relation of the LSM_{11} mode, and for both modes the present method shows an error at least one order of magnitude smaller (in [8] a similar accuracy with the transversal-field method is obtained using 64 first-order triangular elements).

A property of considerable importance in any finite-element method is the convergence of the solution as the problem size increases. Here, the convergence rate, m, of the relative error, e, of the propagation constant as a function of the number of nodal points, N_p, in the finite-element mesh is studied, assuming that $|e| \propto (N_p)^{-m}$ for large enough N_p.

In Fig. 4, $|e|$ is plotted as a function of the number of nodal points, using square first-order elements, for the two modes considered above. For both modes, the present method is found to converge at least quadratically ($m > 2$) as on the other hand the transversal field method only converges linearly ($m \approx 1$). The present method usually predicts a too high $|\beta'|$, in contrast to the transversal field method, where the predicted values usually are too low.

B. Lossy Dielectric-Filled Rectangular Waveguide

This example consists of a waveguide of dimensions $a\times2a$ filled with a lossy dielectric of complex permittivity $\epsilon = 1.5 - j0.15$. The relative errors of the real and imaginary parts of the propagation constant for the fundamental TE_{10} and first higher order TE_{01} modes are compared to the exact solution [13] in Fig. 5(a) and (b) as a function of the number of nodal points using square first-order elements. For comparison, the present results are also compared to the results obtained by the ***H***-field method [9], where triangular second-order elements were used. This comparison is made with respect to the number of nodal points and should be to the favor of the method using second-order elements as the higher order elements are commonly believed to improve the accuracy versus number of nodal points figure (though reducing the matrix sparsity). In any case, it shows that the convergence of the present method also for this structure is roughly quadratic for both modes, while the other method only converges roughly linearly. The predicted value of $|\beta''|$ is usually too low when compared to the exact solution (cf. the real part above).

C. Hollow Circular Waveguide

To confirm the applicability of the present method to curved boundaries, a hollow circular waveguide of radius a

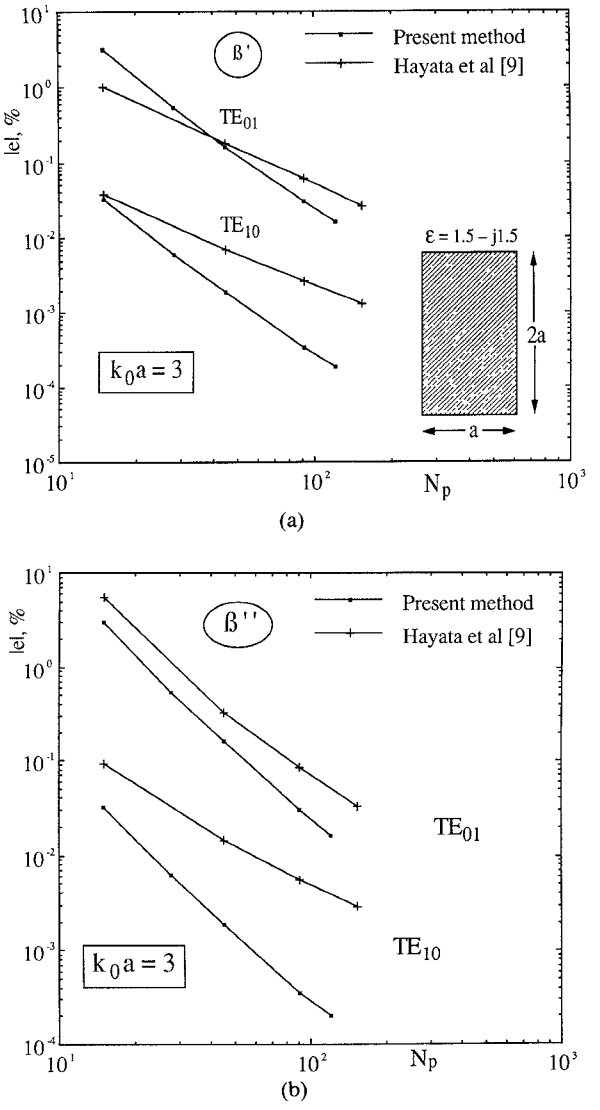

Fig. 5. (a) The relative error in the finite-element solutions of the real part of the propagation constant, β', for the fundamental TE_{10} and the higher order TE_{01} modes in the lossy dielectric-loaded rectangular waveguide (inset) as a function of the number of nodal points, using square first-order elements. (b) The relative error in the imaginary part, β'', of the propagation constant corresponding to errors in the real part shown in Fig. 5(a).

is analyzed using first-order triangular elements. Dispersion relations for the three lowest propagating modes are given in Fig. 6. In this example, one quarter of the waveguide has been divided into 36 first-order ordinary triangular elements utilizing the inherent symmetry for the different modes. The accuracy of the higher order modes can, of course, be improved by increasing the number of elements or by using higher order interpolation on each element. Thus, the applicability of the present method is also demonstrated for the case of curved boundaries, and the accuracy is shown to be retained when using the triangular finite elements.

Also for this case, predicted values of $|\beta'|$ and $|\beta''|$ are usually found to be, respectively, too high and too low. This is analogous to a prediction of β^2 that is too high or, equivalently, a prediction of the transversal wavenumber k_T^2 that is too low. A disadvantage related to this fact is

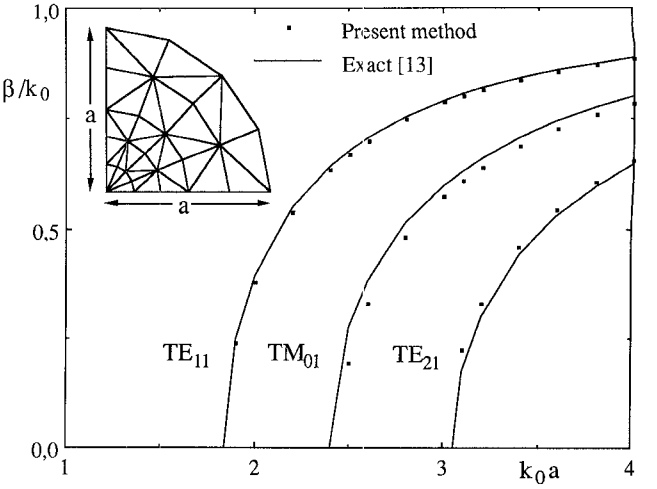

Fig. 6. The propagation characteristics of a hollow circular waveguide, as obtained by the presented method using a mesh (inset) consisting of 36 first-order elements. At the external boundary, Γ, the normal magnetic induction field, B_r, and the tangential electric field, E_ϕ and E_z, are forced to vanish.

that some of the higher order modes, which actually are cut off, are predicted to have $|\beta'| > 0$, and thus get mixed with the propagating modes in the calculated $\beta'(\omega)$ spectrum. However, the former modes seem to be identified by possessing normalized residuals, according to (1a) and (1b), which are higher than for the latter modes.

D. Anisotropic Slab with Dielectric and Magnetic Losses

As a more advanced example relating to the material properties, an anisotropic slab with both dielectric and magnetic losses is studied to verify the general validity of the present method. It consists of a rectangular waveguide of dimensions $a \times 2a$ loaded at one end with an anisotropic slab of dimensions $a \times a$. The slab has the relative scalar permittivity $\epsilon = 2 - j0.2$ and the relative tensor permeability

$$\hat{\mu} = \begin{pmatrix} 1 - j0.1 & 0 & 0.05 - j0.5 \\ 0 & 1 - j0.1 & 0 \\ -0.05 + j0.5 & 0 & 1 - j0.1 \end{pmatrix}.$$

For the fundamental TE_{10} and higher order TE_{20} modes, a division in 1×8 first-order elements gives the complex dispersion relations shown in Fig. 7, where the exact solutions, attainable from the characteristic equation in [13], also are plotted. The correspondence is very good along the whole frequency axis. Note that only eight first-order rectangular elements are used for both the real and imaginary parts of the propagation constants.

The corresponding convergence rates are found in Fig. 8, where square first-order elements have been used to calculate the relative errors in the real and imaginary parts of the complex propagation constant, for modes propagating in both the positive and negative z direction. The resulting convergence order is approximately $m \approx 2.5$ for both modes.

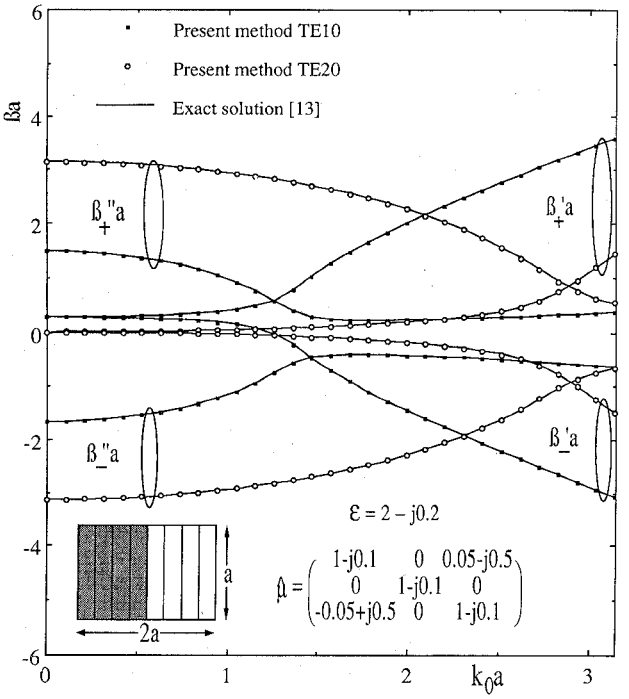

Fig. 7. Complex propagation characteristics for the fundamental TE_{10} and higher order TE_{20} modes in the magnetically anisotropic, magnetically and electrically dissipative slab-loaded rectangular waveguide (inset). The + and − indices denote modes propagating in, respectively, the positive and negative z directions.

V. Conclusion

An advantageous finite-element method for the metal waveguide problem has been developed by which complex propagation characteristics may be obtained for arbitrarily shaped waveguides of arbitrary composition. The method is based on a straightforward application of the Galerkin method to the first-order Maxwell curl equations and comprises all six field components of the electric and magnetic fields. All the necessary boundary conditions on the tangential field components, and additionally on the normal components, are enforced, thus making the final problem size of the same order, or lower, than for comparable formulations.

With the presented method, no spurious modes have been observed, and it has been found to possess very good accuracy and convergence properties in a number of examples that have been analyzed using both rectangular and triangular first-order finite elements. Especially when using the first-order triangular elements, high-order cutoff modes are found with real propagation constants, as the square of the propagation constant is usually predicted too high with the present formulation. However, by calculating the normalized residuals of the solutions, the modes of interest seem to be identified as having the smallest residuals, and are hence separated from the ones with larger residuals.

A very important property of the presented formulation is that the resulting eigenvalue problem is of the sparse type, suitable for large-size problems, and that it is possible to treat both the propagation constant and the frequency as an eigenvalue. The resulting matrix equation may be reformulated in terms of fewer than six field components, and for some usual cases, the final problem size may be reduced by a factor of up to 3.

The extension to higher order elements is straightforward, and by modifications of the method it is possible to treat other types of waveguides as well, e.g. dielectric waveguides with impedance walls and open unbounded dielectric waveguides properly treating the region of infinity.

Appendix

The submatrices in (14) are found from (8)–(10) to be

$$[P_1] = k_0 Z_0 \sum_e \iint_e \begin{bmatrix} \epsilon_{xx}[A] & \epsilon_{xy}[A] \\ \epsilon_{yx}[A] & \epsilon_{yy}[A] \end{bmatrix} dx\,dy \tag{A1}$$

$$[P_2] = k_0 Z_0 \sum_e \iint_e \begin{bmatrix} j\epsilon_{xz}[A] \\ j\epsilon_{yz}[A] \end{bmatrix} dx\,dy \tag{A2}$$

$$[P_3] = k_0 Z_0 \sum_e \iint_e \begin{bmatrix} -j\epsilon_{zx}[A] & -j\epsilon_{zy}[A] \end{bmatrix} dx\,dy \tag{A3}$$

$$[P_4] = k_0 Z_0 \sum_e \iint_e [\epsilon_{zz}[A]]\, dx\,dy \tag{A4}$$

$$[P_5] = k_0 Z_0 \sum_e \iint_e \begin{bmatrix} \mu_{xx}[A] & \mu_{xy}[A] \\ \mu_{yx}[A] & \mu_{yy}[A] \end{bmatrix} dx\,dy \tag{A5}$$

$$[P_6] = k_0 Z_0 \sum_e \iint_e \begin{bmatrix} j\mu_{xz}[A] \\ j\mu_{yz}[A] \end{bmatrix} dx\,dy \tag{A6}$$

$$[P_7] = k_0 Z_0 \sum_e \iint_e \begin{bmatrix} -j\mu_{zx}[A] & -j\mu_{zy}[A] \end{bmatrix} dx\,dy \tag{A7}$$

$$[P_8] = k_0 Z_0 \sum_e \iint_e [\mu_{zz}[A]]\, dx\,dy \tag{A8}$$

$$[R_1] = Z_0 \sum_e \iint_e \begin{bmatrix} -[C] \\ [B] \end{bmatrix} dx\,dy \tag{A9}$$

$$[R_2] = Z_0 \sum_e \iint_e \begin{bmatrix} -[C] & [B] \end{bmatrix} dx\,dy \tag{A10}$$

$$[R_3] = Z_0 \sum_e \iint_e \begin{bmatrix} [C] \\ -[B] \end{bmatrix} dx\,dy \tag{A11}$$

$$[R_4] = Z_0 \sum_e \iint_e \begin{bmatrix} [C] & -[B] \end{bmatrix} dx\,dy \tag{A12}$$

$$[Q_1] = Z_0 \sum_e \iint_e \begin{bmatrix} [0] & -[A] \\ [A] & [0] \end{bmatrix} dx\,dy \tag{A13}$$

$$[Q_2] = Z_0 \sum_e \iint_e \begin{bmatrix} [0] & [A] \\ -[A] & [0] \end{bmatrix} dx\,dy \tag{A14}$$

where the handling of boundary conditions, inherent in each summation symbol, depends on the origin of each of the submatrices in (8)–(10), i.e., on the relation between local and global variables obtained from (2a)–(2h). Thus, Σ_e in (A8) should incorporate the boundary conditions

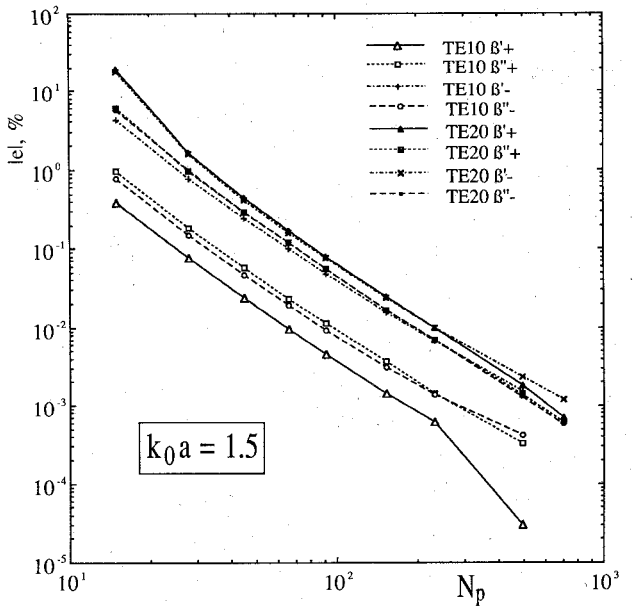

Fig. 8. The relative error in the finite-element solutions of β' and β'' corresponding to the modes in Fig. 7 as a function of the number of nodal points, using square first-order elements.

relating disjoint [11] variables for H_z ($4N$ if N first-order rectangular elements) to conjoint variables for H_z ($= N_{Hz} \approx N$), in what concerns both the row and column entries. Thus $[P_8]$ is a quadratic matrix of dimensions $N_{Hz} \times N_{Hz}$, and the other matrices are obtained in analogous fashion if for each row and column entry the appropriate boundary conditions between disjoint and conjoint variables are considered.

References

[1] Z. J. Csendes, P. Silvester, "Numerical solution of dielectric loaded waveguides: I—Finite-element analysis," *IEEE Trans. Microwave Theory Tech.*, vol. MTT-18, pp. 1124–1131, Dec. 1970.

[2] A. Konrad, "Vector variational formulation of electromagnetic fields in anisotropic media," *IEEE Trans. Microwave Theory Tech.*, vol. MTT-24, pp. 553–559, Sept. 1976.

[3] C. Yeh, S. B. Dong, and W. P. Brown, "Single-mode optical waveguide," *Appl. Opt.*, vol. 18, pp. 1490–1504, May 1979.

[4] B. M. A. Rahman and J. B. Davies, "Penalty function improvement of waveguide solution by finite elements," *IEEE Trans. Microwave Theory Tech.*, vol. MTT-32, pp. 922–928, Aug. 1984.

[5] M. Hano, "Finite-element analysis of dielectric-loaded waveguides," *IEEE Trans. Microwave Theory Tech.*, vol. MTT-32, pp. 1275–1279, Oct. 1984.

[6] M. Koshiba and M. Suzuki, "Finite-element analysis of *H*-plane waveguide junction with arbitrarily shaped ferrite post," *IEEE Trans. Microwave Theory Tech.*, vol. MTT-34, pp. 103–109, Jan. 1986.

[7] K. Hayata, M. Koshiba, M. Eguchi, and M. Suzuki, "Vectorial finite-element method without any spurious solutions for dielectric waveguiding problems using transverse magnetic-field component," *IEEE Trans. Microwave Theory Tech.*, vol. MTT-34, pp. 1120–1124, Nov. 1986.

[8] T. Angkaew, M. Matsuhara, and N. Kumagai, "Finite-element analysis of waveguide modes: A novel approach that eliminates spurious modes," *IEEE Trans. Microwave Theory Tech.*, vol. MTT-35, pp. 117–123, Feb. 1987.

[9] K. Hayata, K. Miura, and M. Koshiba, "Finite-element formulation for lossy waveguides," *IEEE Trans. Microwave Theory Tech.*, vol. 36, pp. 268–275, Feb. 1988.

[10] I. S. Duff, "Survey of sparse matrix research," *Proc. IEEE*, vol. 65, pp. 500–535, Apr. 1977.

[11] P. P. Silvester and R. L. Ferrari, *Finite Elements for Electrical Engineers*. Cambridge: Cambridge University Press, 1983.

[12] R. Wait and A. R. Mitchell, *Finite Element Analysis and Applications*. Chichester: John Wiley & Sons Ltd., 1985.

[13] R. E. Collin, *Field Theory of Guided Waves*. New York: McGraw-Hill, 1960.

[14] NAG Fortran Library, Numerical Algorithms Groups Ltd., Oxford, England.

[15] A. D. Berk, "Variational principles for electromagnetic resonators and waveguides," *IRE Trans. Antennas Propagat.*, vol. AP-4, pp. 104–111, Apr. 1956.

[16] W. J. English, "Vector variational solutions of inhomogeneously loaded cylindrical waveguide structures," *IEEE Trans. Microwave Theory Tech.*, vol. MTT-19, pp. 9–18, Jan. 1971.

[17] Y. Satomura, M. Matsuhara, and N. Kumagai, "Analysis of electromagnetic waveguides in anisotropic slab waveguides," *IEEE Trans. Microwave Theory Tech.*, vol. MTT-22, pp. 86–92, Feb. 1974.

[18] K. D. Paulsen, D. R. Lynch, and T. W. Strohbehn, "Three-dimensional finite, boundary, and hybrid element solution for lossy dielectric media," *IEEE Trans. Microwave Theory Tech.*, vol. 36, pp. 682–693, Apr. 1988.

[19] K. Hayata, M. Eguchi, and M. Koshiba, "Finite-element formulation for guided-wave problems using transversal electric field component," *IEEE Trans. Microwave Theory Tech.*, vol. 37, pp. 256–258, Jan. 1989.

✠

Jan A. M. Svedin (S'88) was born in Skellefteå, Sweden, on November 4, 1962. He received the M.Sc. degree in applied physics and electrical engineering in 1986 from the Linköping Institute of Technology, Linköping, Sweden.

Since 1987, he has been working as a research officer in the Division of Microwave Technology, Department of Information Technology, Swedish Defence Research Establishment, on the field analysis and design of dielectric resonator oscillators, microstrip antenna arrays, and ferrite control components. In addition, he is currently working toward the Ph.D. degree in theoretical physics at the Linköping Institute of Technology.